The astrin–kinastrin/SKAP complex localizes to microtubule plus ends and facilitates chromosome alignment

Anja K. Dunsch, Emily Linnane, Francis A. Barr, and Ulrike Gruneberg

Cancer Research UK Centre, University of Liverpool, Liverpool L3 9TA, England, UK

Astrin is a mitotic spindle–associated protein required for the correct alignment of all chromosomes at the metaphase plate. Astrin depletion delays chromosome alignment and causes the loss of normal spindle architecture and sister chromatid cohesion before anaphase onset. Here we describe an astrin complex containing kinastrin/SKAP, a novel kinetochore and mitotic spindle protein, and three minor interaction partners: dynein light chain, Plk1, and Sgo2. Kinastrin is the major astrin-interacting protein in mitotic cells, and is required for astrin targeting to microtubule plus ends proximal to the plus tip tracking protein EB1. Cells overexpressing or depleted of kinastrin mislocalize astrin and show the same mitotic defects as astrin-depleted cells. Importantly, astrin fails to localize to and track microtubule plus ends in cells depleted of or overexpressing kinastrin. These findings suggest that microtubule plus end targeting of astrin is required for normal spindle architecture and chromosome alignment, and that perturbations of this pathway result in delayed mitosis and nonphysiological separase activation.

Introduction

Successful cell division requires the formation of a bipolar spindle with sister chromatids stably attached to spindle microtubules (MTs) from opposite poles. Sister chromatids bind to MTs via their kinetochores, proteinaceous structures that are formed in mitosis on the centromeres (Cheeseman and Desai, 2008; Santaguida and Musacchio, 2009). Kinetochores that are not correctly attached generate a signal that activates the spindle assembly checkpoint (SAC) and thus prevents entry into anaphase. Once bipolar attachment and alignment of chromosomes at the metaphase plate are achieved, the cohesion between sister chromatids is abolished by the action of the protease separase, and chromosome segregation ensues (Uhlmann et al., 2000).

Recent studies suggest that MTs bind kinetochores via multiple weak attachments (Cheeseman and Desai, 2008; Santaguida and Musacchio, 2009; McEwen and Dong, 2010). The key MT attachment complex at the kinetochore is comprised of the KNL-1, Mis12, and Ndc80 protein subcomplexes (Cheeseman et al., 2006). Interference with these proteins abolishes MT–kinetochore attachments. Other kinetochore components,

such as the motor proteins CenpE and dynein, MT plus end binding factors including EB1 and CLIP-170, the Ska complex, and CenpF also interact directly with MTs and aid the formation of stable MT–kinetochore attachments (Cheeseman and Desai, 2008; Santaguida and Musacchio, 2009). In addition, spindle-associated proteins such as astrin contribute to the fidelity of chromosome alignment and mitotic progression (Thein et al., 2007). However, both the molecular function of astrin and the basis for its targeting to the mitotic spindle remain unclear.
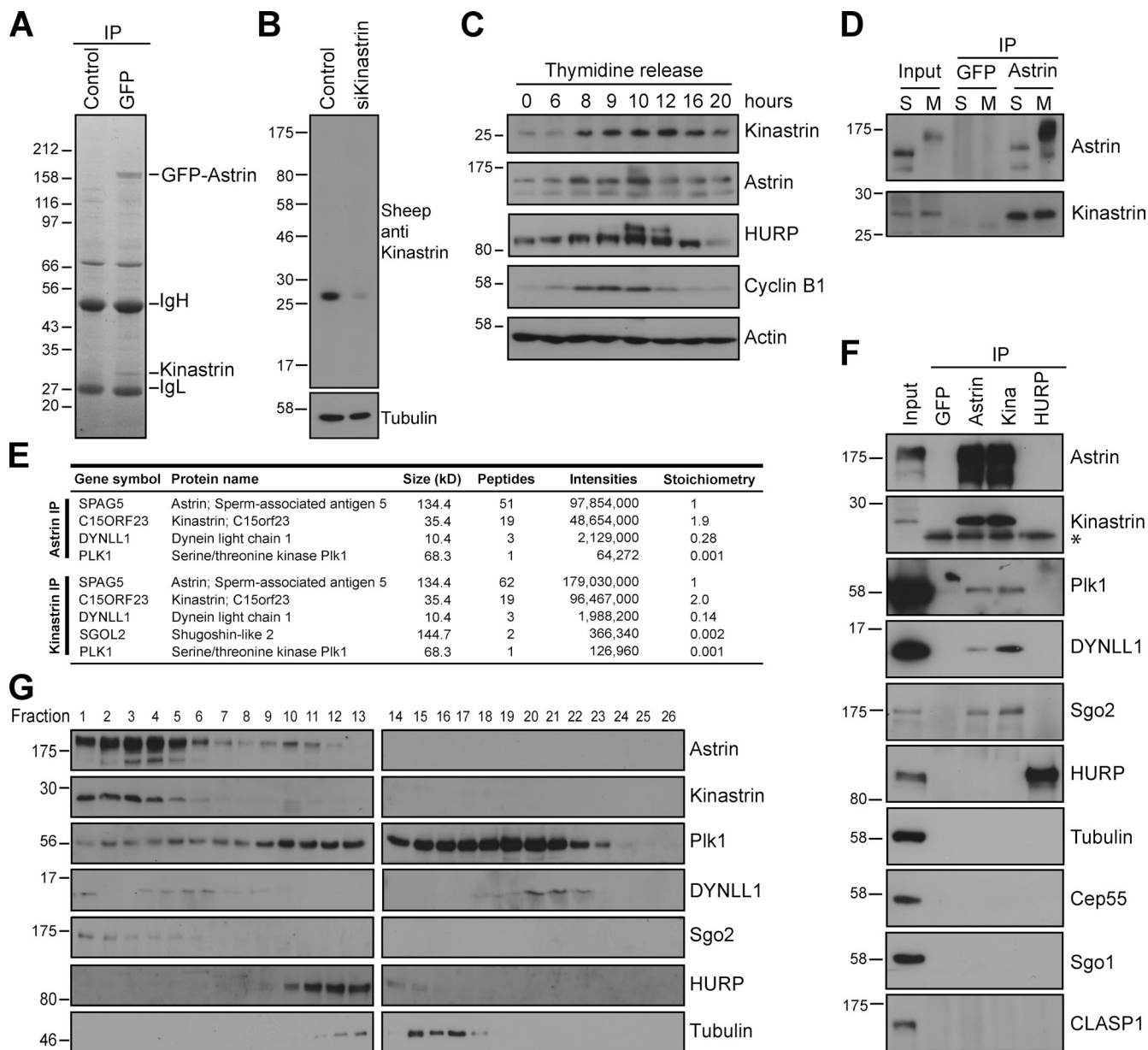
Results and discussion

Identification of the astrin–kinastrin/SKAP complex

To identify novel interaction partners of astrin, GFP–astrin complexes purified from mitotic HeLa cells stably expressing GFP–astrin were analyzed by SDS-PAGE and mass spectrometry (Fig. 1 A and Fig. S1, A and B). The two major Coomassie-stained bands at 160 kD and 30 kD were identified as astrin and

Correspondence to Ulrike Gruneberg: u.gruneberg@liv.ac.uk

Abbreviations used in this paper: HURP, hepatoma up-regulated protein; MT, microtubule; SAC, spindle assembly checkpoint; SKAP, small kinetochore-associated protein.

The Rockefeller University Press $30.00
J. Cell Biol. Vol. 192 No. 6   959–968
www.jcb.org/cgi/doi/10.1083/jcb.201008023

JCB   959

E

	Gene symbol	Protein name	Size (kD)	Peptides	Intensities	Stoichiometry
Astrin IP	SPAG5	Astrin; Sperm-associated antigen 5	134.4	51	97,854,000	1
	C15ORF23	Kinastrin; C15orf23	35.4	19	48,654,000	1.9
	DYNLL1	Dynein light chain 1	10.4	3	2,129,000	0.28
	PLK1	Serine/threonine kinase Plk1	68.3	1	64,272	0.001
Kinastrin IP	SPAG5	Astrin; Sperm-associated antigen 5	134.4	62	179,030,000	1
	C15ORF23	Kinastrin; C15orf23	35.4	19	96,467,000	2.0
	DYNLL1	Dynein light chain 1	10.4	3	1,988,200	0.14
	SGOL2	Shugoshin-like 2	144.7	2	366,340	0.002
	PLK1	Serine/threonine kinase Plk1	68.3	1	126,960	0.001

Figure 1. **Kinastrin/SKAP is a novel astrin interaction partner.** (A) Astrin complexes were immunoprecipitated from mitotic extracts of HeLa S3 GFP–astrin cells with anti-GFP or control anti-GST antibodies. The isolated complexes were separated on a 4–12% NuPAGE gel and analyzed by nano–LC-MS/MS. (B) Extracts of control or kinastrin-depleted cells were Western blotted with affinity-purified sheep anti-kinastrin antibodies. (C) HeLa S3 cells were synchronized with a double thymidine release protocol. Samples were taken at the indicated time points and Western blotted as shown. (D) Astrin immunoprecipitates from HeLa cells arrested in interphase/S phase or M phase were Western blotted with astrin and kinastrin antibodies. (E and F) Astrin, kinastrin, HURP, or GFP (control) immunoprecipitates from mitotic HeLa S3 extracts were analyzed by quantitative nano–LC-MS/MS (E) or Western blotted as indicated (F). The asterisk indicates an Ig light chain. (G) Mitotic cell extracts were separated using a Superose 6 10/300 GL column (GE Healthcare) and Western blotted as shown. Numbers next to gel blots indicate molecular mass in kilodaltons.

kinastrin/SKAP/C15orf23, respectively (Fig. 1 A). Kinastrin/SKAP/C15orf23 is present in a published total spindle proteome (Sauer et al., 2005) and *C15ORF23* was recently identified as a G2-induced gene endoding the small kinetochore-associated protein (SKAP; Whitfield et al., 2002; Fang et al., 2009), which supports the idea that it may be an important mitotic partner for astrin. For further analysis, specific antibodies to kinastrin were generated. Western blot analysis of control or kinastrin-depleted cell extracts demonstrated that a single band of the expected molecular weight was detected, the

intensity of which was significantly reduced by kinastrin depletion (Fig. 1 B). Western blotting of synchronized cell extracts revealed that kinastrin protein levels increased and decreased as cells entered and exited mitosis (Fig. 1 C), which confirms that kinastrin is a mitotically regulated protein (Whitfield et al., 2002; Fang et al., 2009). Similar behavior was observed for astrin and the unrelated mitotic spindle regulator hepatoma upregulated protein (HURP; Fig. 1 C; Koffa et al., 2006; Silljé et al., 2006). To confirm that endogenous astrin and kinastrin form a complex, reciprocal immunoprecipitations were performed

(Fig. 1, D–F; and Fig. S1 C). Western blot analysis showed that astrin and kinastrin coprecipitated in both interphase and mitosis, whereas other spindle and kinetochore proteins such as HURP, tubulin, Cep55, and CLASP1 (Maffini et al., 2009) did not (Fig. 1, D and F). Analysis of these complexes using label-free quantitative liquid chromatography/tandem mass spectrometry (LC-MS/MS) revealed that astrin and kinastrin were the major components present, and that the apparent stoichiometry of the astrin–kinastrin complex was 1:2, which suggests that two molecules of kinastrin interact with one molecule of astrin (Fig. 1 E). This analysis also revealed minor interaction partners of the astrin–kinastrin complex, namely Polo-like kinase 1 (Plk1), Shugoshin-like protein 2 (Sgo2), and dynein light chain (DYNLL1; Fig. 1 E). In agreement with the mass spectrometry data, Western blotting revealed that Plk1, DYNLL1, and Sgo2, but not Sgo1, readily precipitated with astrin and kinastrin but not with HURP (Fig. 1 F). Gel filtration analysis of mitotic cell extracts demonstrated the presence of astrin and kinastrin, as well as Plk1, Sgo2, and DYNLL1 in the same high molecular weight fractions, which indicates that these proteins may be part of a large protein complex (Fig. 1 G). Collectively, our findings suggest that Plk1, DYNLL1, and Sgo2 may be bona fide regulators of the astrin–kinastrin complex.

Kinastrin is a mitotic spindle protein

Co-staining of HeLa cells in different stages of mitosis with antibodies against kinastrin and astrin showed that both are present at kinetochores and spindle poles (Fig. 2 A), leading us to name this novel astrin interaction partner kinastrin (kinetochore-localized astrin-binding protein). Transfection of HeLa cells for 72 h with four individual siRNA duplexes targeting C15orf23 reduced kinastrin levels measured by either Western blotting or immunofluorescence (Fig. 2 B and Fig. S1, E and F). For further analysis of kinastrin, siRNA duplex 5 was used. Strikingly, kinastrin-depleted cells often exhibited multipolar spindle structures with disorganized chromatin, which is reminiscent of astrin depletion (Fig. 2 B and Fig. S1 E). Furthermore, kinastrin and astrin depletion resulted in both loss of the respective interaction partner from the spindle and kinetochores and reduced protein levels in the extracts (Fig. 2 B). This suggests that astrin and kinastrin target to the kinetochores and spindle poles as a complex. Live cell imaging of kinastrin-depleted cells confirmed that loss of kinastrin resulted in the same phenotype as astrin depletion, specifically delayed chromosome alignment and arrest in mitosis as well as loss of both normal spindle architecture and chromatin organization (Fig. 2, C and D). Of the 51 kinastrin-depleted cells analyzed, 59% exhibited delayed chromosome congression, whereas 41% never aligned their chromosomes. The majority of cells with a congression phenotype eventually progressed into anaphase (33% of total), whereas the rest remained arrested in mitosis until the end of the experiment. Strikingly, 31% of all cells displayed strongly disorganized spindle structure and chromatin organization shortly after entering mitosis (Fig. 2 C). All mitotically arrested kinastrin-depleted cells exhibited persistent SAC signaling (Fig. 2, E and F) and were strongly positive for securin and cyclin B1 (unpublished data). In summary, our data suggest that kinastrin is an

essential component of the mitotic spindle required for normal chromosome segregation and progression into anaphase.

Characterization of astrin–kinastrin complex architecture

To understand how astrin and kinastrin target to the spindle, the interaction domains in the two proteins were mapped. This revealed that the C-terminal region of astrin, comprising amino acids 482–850, is sufficient to bind kinastrin (Fig. 3 A). Interestingly, this is also the minimal MT-binding domain identified in astrin (Fig. 3 A, immunofluorescence panel), which implies that astrin localizes to MTs through kinastrin. The minimal astrin-binding site in kinastrin was mapped to amino acids 159–317, and this was also the minimal region required for kinastrin spindle localization (Fig. 3 B). Interestingly, high expression levels of kinastrin fragments capable of interacting with astrin resulted in reduced levels of astrin on the spindle and kinetochores (Fig. 3 B). These cells typically showed disturbed spindle structure and disorganized chromatin similar to the astrin depletion phenotype (Fig. 3 B). Elevated levels of kinastrin may therefore exert a dominant-negative effect on astrin, perhaps by saturating the spindle-binding sites for the astrin–kinastrin complex.
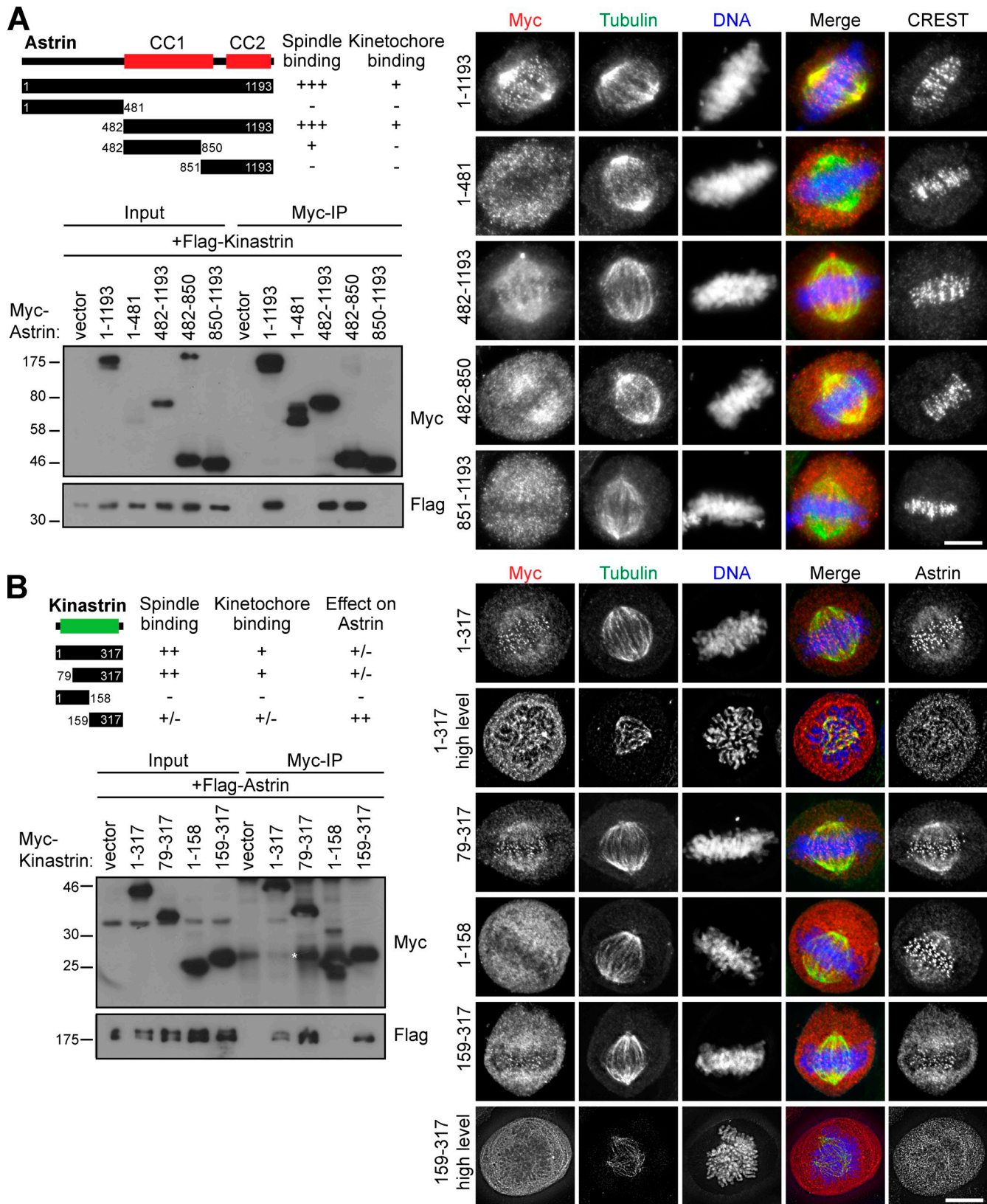
Astrin localization to the spindle poles and kinetochores is required for normal mitotic progression

Kinastrin overexpression displaces endogenous astrin–kinastrin complexes from the spindle, and therefore allowed the function of the spindle-targeted pool of astrin to be examined. Stable cell lines expressing doxycycline-inducible Myc-kinastrin were generated for this purpose. Induction of Myc-kinastrin expression for 24 h resulted in a dramatic increase in mitotic cells with multipolar spindles (Fig. 4 A and Fig. S2 A). Closer examination of these cells showed that the overexpressed Myc-kinastrin accumulated in the cytoplasm, and, as a consequence, astrin was delocalized from the spindle and kinetochores (Fig. 4 A, left immunofluorescence panel, "high"). In contrast, overexpression of Myc-astrin attracted more kinastrin to the spindle poles (Fig. 4 A, right immunofluorescence panel). The disturbed spindle architecture and highly disorganized chromatin structure observed in Myc-kinastrin–overexpressing cells was very similar to the astrin depletion phenotype, albeit with unaltered protein levels of astrin (Fig. 4 A, Western blot). Astrin-depleted cells have previously been shown to display elevated levels of prematurely separated sister chromatids and poles with single centrioles (Thein et al., 2007). This was also observed in Myc-kinastrin–overexpressing cells (Fig. 4, B and C; and Fig. S2 B). Thus, kinastrin overexpression recapitulates the key features of the astrin depletion phenotype (Thein et al., 2007). Together, these findings demonstrate that the correct localization of astrin, and not just its presence, is critical for the timely progression through mitosis and normal entry into anaphase.

Mitotically arrested cells with single centrioles at the poles of multipolar spindles and partially or fully separated sister chromatids were also observed in kinastrin-depleted cells (Fig. 4, D and E; and Fig. S2 C). Both phenotypes may be at least partially caused by aberrant separase activation
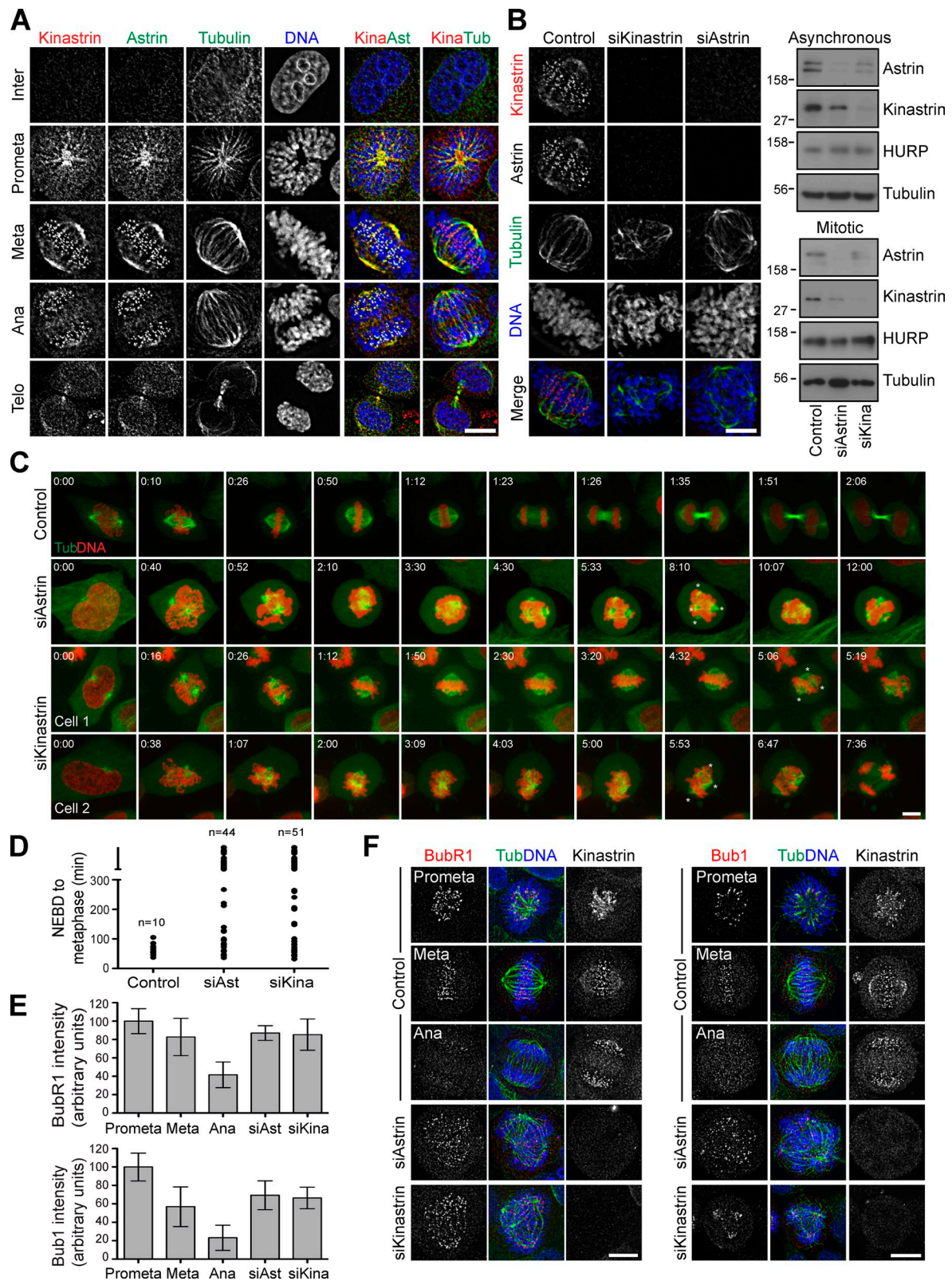
Figure 2. **The astrin–kinastrin complex is required for efficient chromosome alignment and segregation.** (A) HeLa S3 cells were stained with antibodies to kinastrin, astrin, and tubulin. DNA was stained with DAPI. (B) HeLa cells were treated with the indicated siRNAs (astrin for 48 h, kinastrin for 72 h) and stained as in A; or cell extracts were prepared from total cells or mitotic shake-offs and Western blotted with the indicated antibodies. Numbers next to gel blots indicate molecular mass in kilodaltons. Bar, 10 µm. (C and D) HeLa cells stably expressing mCherry-histone H2B and GFP–tubulin were treated with control, astrin, or kinastrin siRNA oligos and synchronized with 2.5 mM thymidine 30 h after siRNA addition. After 20 h, the cells were released, incubated for 8 h at 37°C, and then filmed for 12 h. The time required from nuclear envelope breakdown to metaphase alignment was plotted for control, astrin-depleted, and kinastrin-depleted cells (D). (E and F) Control, astrin-depleted, or kinastrin-depleted HeLa cells were fixed and stained with antibodies against kinastrin and BubR1 (left) or Bub1 (right). The staining intensity was quantified and plotted (E). Error bars indicate the standard error of the mean. Bars, 10 µm.
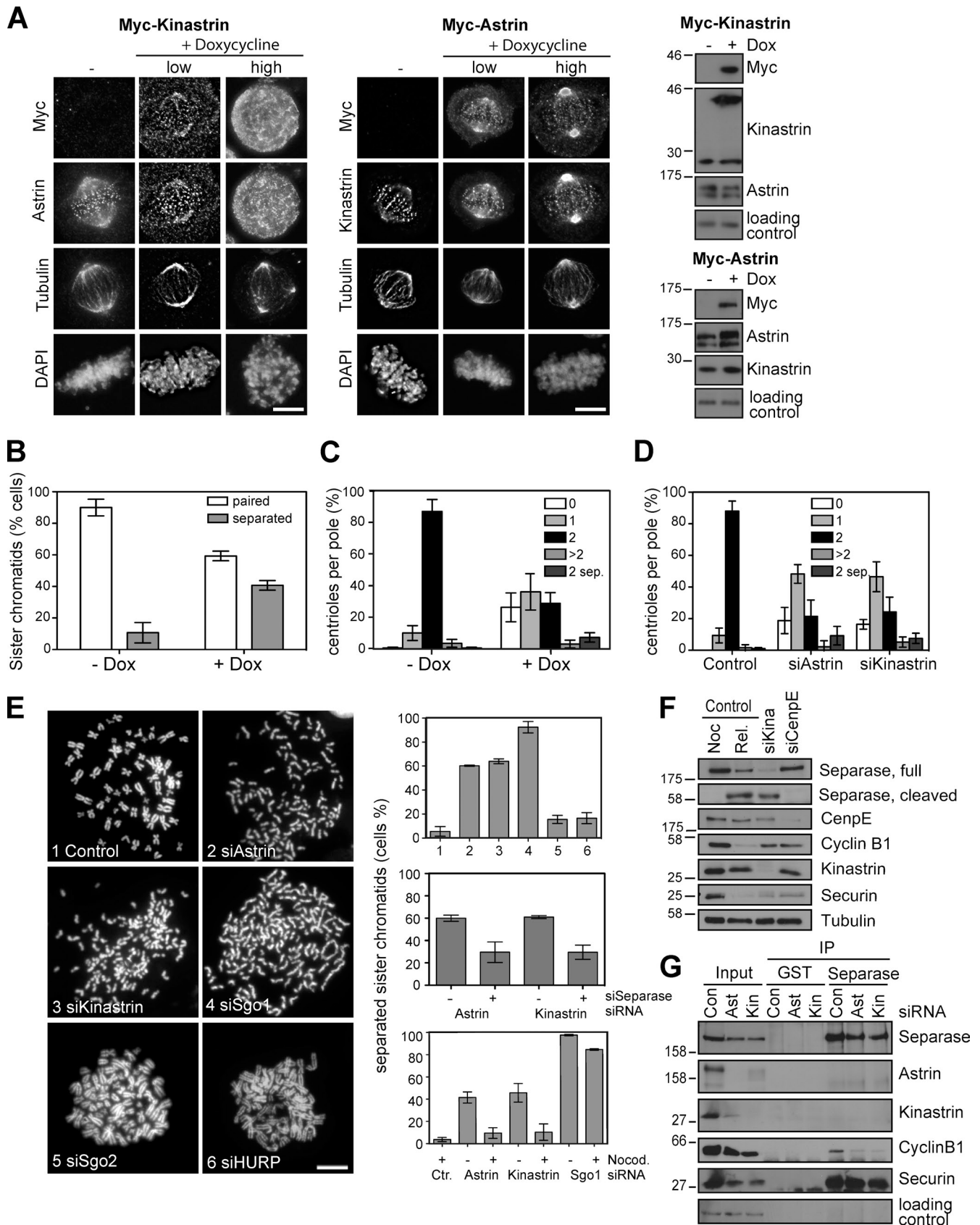
Figure 3.   **Spindle targeting of astrin is mediated through the kinastrin-binding domain.** (A and B) Myc-astrin (A) or Myc-kinastrin fragments (B) alone or in conjunction with FLAG-kinastrin (A) or FLAG-astrin (B) were transiently transfected into HeLa S3 cells for immunofluorescence analysis and HEK 293T cells for immune precipitations. HEK 293T cells were synchronized in mitosis by addition of the Eg5 inhibitor S-trityl-ʟ-cysteine (STLC; 10 µM) for 14 h after 24 h of transfection. The cells were then harvested and lysed, and anti-Myc immunoprecipitations were performed. Western blots were probed as indicated. The asterisk indicates a degradation product. For immunofluorescence analysis, fixed HeLa cells were stained with antibodies to Myc, tubulin, and CREST serum. DNA was stained with DAPI. Numbers next to gel blots indicate molecular mass in kilodaltons. Bars, 10 µm.

Figure 4. **Disrupted astrin function and premature loss of sister chromatid cohesion in kinastrin-depleted or overexpressing cells.** (A) HeLa Flp-in TRex Myc-kinastrin and HeLa Flp-in TRex Myc-astrin cells were mock treated or treated with 1 μg/ml doxycycline for 24 h, then stained for Myc, astrin, kinastrin, and tubulin or harvested for Western blotting with the indicated antibodies. Transfected kinastrin conforms to the longest splice variant of *C15ORF23*. DNA was stained with DAPI. Cells with different expression levels of Myc-kinastrin or Myc-astrin, respectively, are shown. Bar, 10 μm. (B) HeLa Flp-in

(Thein et al., 2007). Consistent with this idea, the separase auto-cleavage fragment of ∼60 kD could be found in kinastrin- but not CenpE-depleted cells, and there was also less separase–cyclin B1 complex in these cells (Fig. 4, F and G). Furthermore, depletion of separase in addition to astrin or kinastrin significantly reduced the amount of premature sister chromatid separation (Fig. 4 E). The addition of nocodazole to astrin- or kinastrin-depleted cells also strongly decreased the occurrence of prematurely separated sister chromatids (Fig. 4 E, bottom graph). This suggests that either spindle pulling forces are required for the separation of the sister chromatids in astrin- or kinastrin-depleted cells, or that hyperactivation of the SAC can suppress the precocious sister chromatid separation. Importantly, the shugoshin pathway for cohesin protection (Kitajima et al., 2006) was not affected by astrin or kinastrin depletion, as Sgo1, Sgo2, and PP2A-B56α were still found at centromeres (Fig. S3). Although separase is unlikely to be directly regulated by astrin or kinastrin, these data suggest that the astrin–kinastrin complex at kinetochores may be required for normal SAC function important for full separase inhibition. A related proposal has been made for the Ska proteins that have been suggested to couple the mechanical sensing of tension to SAC signaling (Daum et al., 2009). In support of this idea, a recent proteomic analysis of chromosomal proteins purified from cells depleted of the Ska complex showed that components of the anaphase-promoting complex/cyclosome were specifically lost from kinetochores (Ohta et al., 2010). Misregulated anaphase-promoting complex/cyclosome function may then follow, and a similar scenario is possible for astrin and kinastrin.

The astrin–kinastrin complex localizes to MT plus ends

To define a molecular basis for the observed phenotypes of defective chromosome congression and disturbed spindle structure, GFP–astrin cells were analyzed in more detail. Imaging of GFP–astrin cells in interphase revealed comet-like structures moving toward the periphery of the cell with a velocity of 0.43 ± 0.05 µm/s (Fig. 5 A and Video 8), which is reminiscent of EB1 MT plus end tracking comets (Akhmanova and Steinmetz, 2008). Indeed, co-staining with antibodies against EB1 as well as live cell imaging of GFP–astrin cells transiently transfected with EB1-mCherry confirmed that GFP–astrin decorated EB1-labeled MTs in both interphase and mitosis, and that the mCherry- and GFP-labeled structures moved together (Fig. 5, B and C; and

Video 9). The GFP–astrin staining was always proximal to the EB1 signal at the MT plus end, which suggests that the features on the MT plus ends recognized by astrin and EB1 are not identical. Endogenous astrin and kinastrin also labeled MT plus ends in a similar manner (Fig. 5 D and not depicted). As expected for MT-associated labeling, both EB1 and GFP–astrin comet staining was lost upon nocodazole treatment (Fig. 5 E). Interphase GFP–astrin comet staining was also lost in the absence of kinastrin, which confirms the idea that astrin localizes to MTs via kinastrin in a manner independent of the cell cycle stage (Figs. 1 D and 5 F).

To test if the astrin–kinastrin complex exerts a direct effect on MT dynamics, in vitro polymerization assays using purified tubulin were performed. Titration of recombinant kinastrin into MT polymerization assays resulted in increased tubulin polymerization (Fig. 5 G), which suggests it may act to stabilize MT plus ends. Altered MT–kinetochore regulation may therefore be the underlying molecular defect resulting in impaired chromosome alignment and spindle integrity in cells with perturbed astrin–kinastrin function. Consistent with this idea, kinastrin-depleted cells were impaired in their ability to reform robust bipolar spindles after combined monastrol and cold treatment (Fig. 5 H), and kinetochore fibers formed in the absence of kinastrin were disorganized and stained less intensely for tubulin compared with control cells (Fig. 5 I).

The astrin–kinastrin complex promotes stable MT–kinetochore attachments

We have characterized kinastrin/SKAP/C15orf23, an astrin partner protein with an identical cellular localization to astrin. Like astrin, kinastrin is required for chromosome alignment, normal timing of sister chromatid segregation, and maintenance of spindle pole architecture. Furthermore, astrin and kinastrin form an MT plus end tracking complex that is required for the formation of normal kinetochore fibers (Fig. 5). While this work was under revision, two studies were published that showed that astrin depletion destabilizes kinetochore fibers and that Aurora B inhibition promotes astrin complex localization to the kinetochores (Manning et al., 2010; Schmidt et al., 2010). Our data on the plus end tracking characteristics of astrin–kinastrin provide a molecular explanation for both these findings, as such a complex would be in a good position to stabilize kinetochore fibers and would also accumulate upon the stabilization of MT–kinetochore attachments by Aurora B inhibition. Interestingly, one of the astrin–kinastrin interaction

TRex Myc-kinastrin cells were mock treated and mitotically arrested with 100 ng/ml nocodazole for 14 h or induced with 1 µg/ml doxycycline for 24 h. Chromosome spreads were prepared and the percentage of cells with separated sister chromatids was assessed. (C) HeLa Flp-in TRex Myc-kinastrin cells were treated as in A and stained for centrin-3 and tubulin. The percentages of spindle poles with zero, one, two, more than two, or markedly separated centrioles are plotted in the bar graph. (D) HeLa S3 cells treated with control, astrin, or kinastrin siRNA oligos for 48 or 72 h (kinastrin) were stained as in C. Centriole numbers at the spindle poles are plotted in the bar graph. (E) HeLa S3 cells were transfected with control, astrin, kinastrin, Sgo1, Sgo2, or HURP siRNA duplexes for 48 or 72 h (kinastrin), harvested by mitotic shake-off (control cells were treated with 100 ng/ml nocodazole for 14 h before harvest), and processed for chromosome spreads. 100 cells were counted from each condition (n = 3; top graph, representative images are shown on the left). Depletion of separase in addition to astrin or kinastrin significantly lowered the amount of cells with separated sister chromatids (middle graph). The addition of nocodazole to astrin- or kinastrin-depleted cells released from a thymidine block significantly reduced the amount of premature loss of sister chromatid cohesion (bottom graph). (F) HeLa cells arrested in mitosis with nocodazole, released from the nocodazole block, or treated with siRNAs targeting CenpE (48 h) or kinastrin (72 h) were harvested by mitotic shake-off (except nocodazole release), then lysed and blotted with the indicated antibodies. Note that kinastrin-depleted cells have cyclin B1 and securin levels lower than nocodazole-arrested cells but comparable to CenpE-depleted cells. The separase cleavage fragment, however, only appears in kinastrin-depleted cells. (G) Separase immunoprecipitations from HeLa cells depleted of astrin or kinasterin for 48 or 72 h were blotted as indicated. All error bars indicate the standard error of the mean. Numbers next to gel blots indicate molecular mass in kilodaltons.
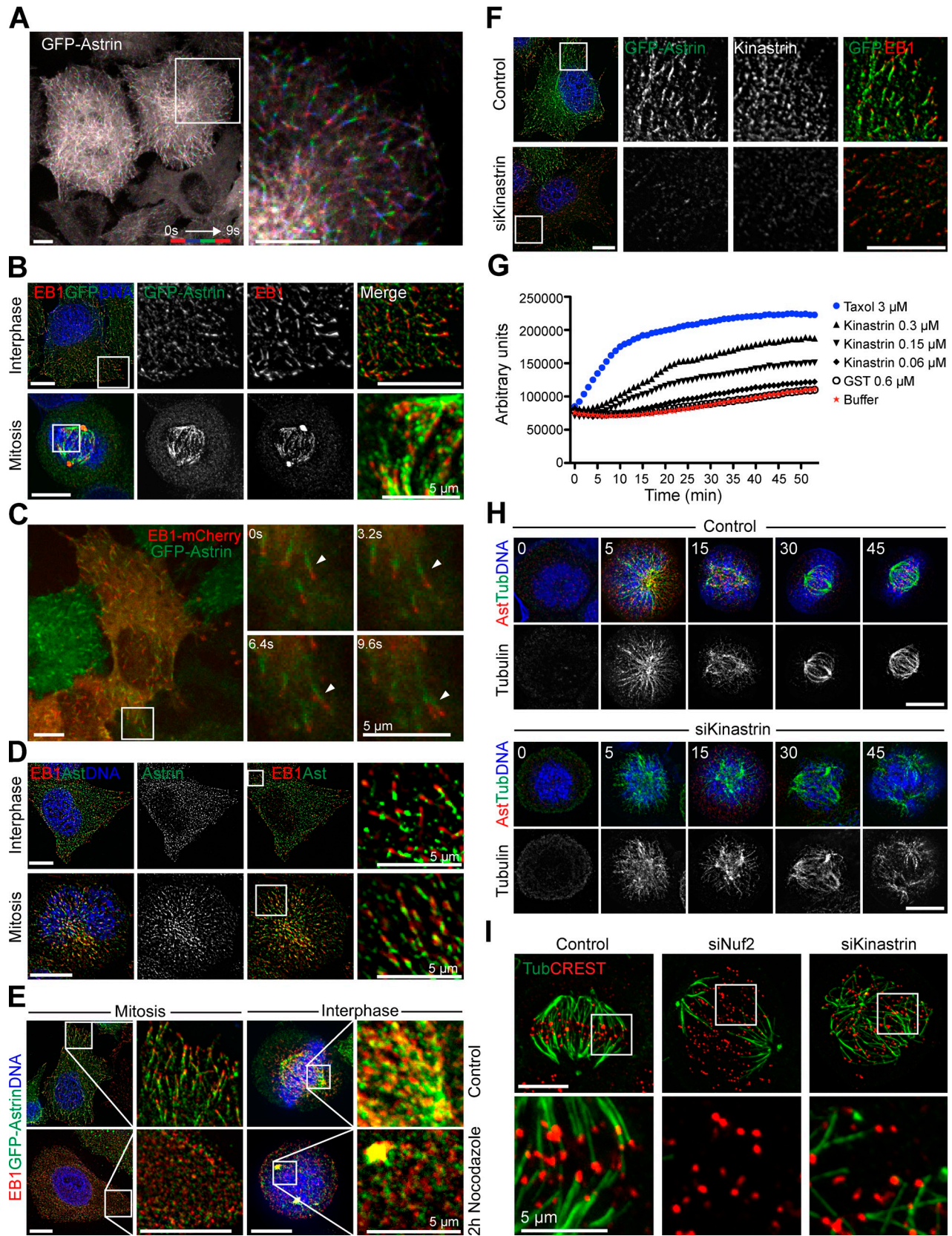
Figure 5. The astrin-kinastrin/SKAP complex localizes to MT plus ends. (A) GFP–astrin cells were imaged every 1.25 s. The first, third, fifth, and seventh frames were projected into one image using different colors as indicated. (B) Methanol-fixed GFP–astrin cells were stained for EB1 and GFP. (C) GFP–astrin cells transiently expressing EB1-mCherry were imaged every 3.2 s. The arrowheads indicate one growing MT plus end that can be followed through the different frames of the movies. (D) Methanol-fixed HeLa cells were stained for astrin and EB1. Single focal planes are shown. (E) GFP–astrin cells were mock-treated or treated with 100 ng/ml nocodazole for 2 h, then stained with CREST antiserum and for EB1 and GFP. (F) GFP–astrin cells were treated

partners that we identified is the dynein light chain DYNLL1, one of three different dynein light chains found in cytoplasmic dynein (Fig. 1, E and F; Pfister et al., 2005, 2006). Dynein has been implicated in chromosome alignment, the formation of MT–kinetochore attachments, and SAC silencing, and has also been found to localize to MT plus ends (Kobayashi and Murayama, 2009; Bader and Vaughan, 2010). Other dynein-associated complexes, such as dynactin, associate with MT plus ends, and this may be important for MT search–capture functions (Echeverri et al., 1996; Varma et al., 2008). Although the precise interplay between the astrin–kinastrin/SKAP complex and dynein is currently unclear, it is conceivable that this complex promotes dynein-mediated transport from MT plus ends toward spindle poles of factors, such as Spindly, required to promote timely chromosome congression and attachment, and spindle checkpoint regulation (Chan et al., 2009; Barisic et al., 2010; Gassmann et al., 2010).

Materials and methods

Antibodies
Hexahistidine-tagged C-astrin aa 1,014–1,193 and C15orf23/kinastrin/SKAP were expressed in and purified from bacteria. Antibodies against C-astrin and full-length kinastrin/SKAP were raised in sheep (Scottish National Blood Transfusion Service) and affinity-purified using the His-tagged proteins coupled to Affigel-15 (Bio-Rad Laboratories). For Western blotting after immunoprecipitation, biotinylated anti-kinastrin antibodies were used in some experiments. Other antibodies were as follows: mouse anti–actin-HRP (Abcam), rabbit anti-astrin (Thein et al., 2007), mouse anti-B56α (BD), mouse anti-Bub1 (Abcam), mouse anti-BubR1 (Millipore), mouse anti-centrin-3 (Abcam), sheep anti-Cep55 (Bastos and Barr, 2010), rabbit anti-CLASP1 (Bethyl Laboratories, Inc.), CREST autoimmune serum (Europa Biosciences), mouse anti-cyclin B1 (Millipore), rabbit anti-CenpE (Bethyl Laboratories, Inc.), rabbit anti-DYNLL1 (Epitomics, Inc.), mouse anti-EB1 (Cell Signaling Technology), rabbit anti-FLAG (Sigma-Aldrich), sheep anti-HURP (a kind gift of J. Harper, Cancer Research Centre, University of Liverpool, England, UK), mouse anti-Myc (clone 9E10), rabbit anti-Myc (both from Sigma-Aldrich), mouse anti-Plk1 (Santa Cruz Biotechnology, Inc.), mouse anti-PPP2CA (BD), mouse anti-Sgo1 (Abcam), rabbit anti-Sgo2 (Bethyl Laboratories, Inc.), mouse anti-securin (Bethyl Laboratories, Inc.), mouse anti-separase (Abcam), rabbit anti-separase (Bethyl Laboratories, Inc.), mouse anti–α-tubulin (clone DM1A; Sigma-Aldrich), and rabbit anti-tubulin (Epitomics, Inc.). Secondary antibodies conjugated to HRP or Cy5 were obtained from Jackson ImmunoResearch Laboratories, Inc. Secondary antibodies conjugated to Alexa Fluor 488, 555, and 647 were obtained from Invitrogen. DNA was stained with DAPI (Sigma-Aldrich).

Molecular biology
C15ORF23 transcript variant 1 and EB1 were amplified from Marathon human testis cDNA (Takara Bio, Inc.) using Pfu polymerase (Agilent Technologies). Full-length astrin constructs have been described previously (Thein et al., 2007). C15ORF23, astrin fragments, and EB1 expression constructs were generated using pcDNA3.1 and pcDNA5/FRT/TO vectors (Invitrogen) modified to encode N-Myc, N-FLAG, or C-mCherry tags, respectively. For bacterial expression, C15ORF23 was cloned into pGEX-5X-1 (GE Healthcare). GST and GST–kinastrin were purified according to the manufacturer's recommendations.

Cell lines
HeLa S3 cells stably expressing GFP–astrin were generated using standard procedures and selected with 0.7 mg/ml geneticin. Stable cell lines with single copies of the desired transgene were created using the TRex inducible

Flp-In system (Invitrogen). HeLa S3 mCherry-histone H2B-tubulin GFP cells were provided by K. Zeng (Cancer Research Centre, University of Liverpool, England, UK; Zeng et al., 2010).

Gel filtration, immunoprecipitations, and protein identification
Samples of mitotic cell extracts separated on a Superose 6 10/300 GL column (GE Healthcare) were provided by R. Nunes-Bastos (Cancer Research Centre, University of Liverpool, Liverpool, England, UK). For immunoprecipitation of GFP–astrin, endogenous astrin, kinastrin/SKAP, or HURP, HeLa S3 cells were arrested in mitosis by addition of 10 µM S-trityl-L-cysteine (Sigma-Aldrich) 14 h before mitotic shake-off. Cell pellets were lysed in lysis buffer (20 mM Tris-Cl, pH 7.4, 150 mM NaCl, 1% IGEPAL, 0.1% sodium deoxycholate, 40 mM β-glycerophosphate, 10 mM NaF, 0.3 mM orthovanadate, 100 nM okadaic acid, and protease inhibitor cocktail [Sigma-Aldrich]) and cleared by centrifugation. Protein complexes were isolated using sheep antibodies against GFP, astrin, kinastrin/SKAP, and HURP bound to protein G–Sepharose and washed with lysis buffer followed by washes in 20 mM Tris-Cl, pH 7.4, 150 mM NaCl, 0.1% IGEPAL, 20 mM Tris-Cl, pH 7.4, and 150 mM NaCl. Protein samples for mass spectrometry were separated on 4–12% gradient NuPAGE gels (Invitrogen), then stained using a colloidal Coomassie blue stain. Gel lanes were cut into 12 slices and then digested with trypsin (Shevchenko et al., 1996). Tryptic peptides were resolved using a 25 cm × 75 µm BEH-C18 column in 0–37.5% acetonitrile in 0.1% formic acid at a flow rate of 400 nl/min with a nanoAcquity ultra performance liquid chromatography device (Waters). Online LC-MS/MS was performed with an Orbitrap XL ETD mass spectrometer (Thermo Fisher Scientific) fitted with a nano-electrospray source (Proxeon) set to acquire an MS survey scan in the Orbitrap (R = 30,000) and then perform MS/MS on the top five multiple-charged ions in the linear quadrupole ion trap after fragmentation using collision ionization (30 ms, 35% energy). Maxquant and Mascot (Matrix Science) were then used to compile and search the raw data against the human International Protein Index database (Cox and Mann, 2008). Protein group and peptide lists were sorted and analyzed in Excel (Microsoft) and Maxquant.

RNA interference
RNA interference using astrin, Sgo1, Gl2 (control), Nuf2 and separase siRNA oligos was performed as described previously (Thein et al., 2007). Kinastrin/SKAP oligos were: No. 1, 5′-CAAACTCGGGCCACTTCTA-dTdT-3′; No. 2, 5′-CAAATGAAAGCTACTGACAdTdT-3′ (Sigma-Aldrich); No. 5, 5′-AGGCTACAAACCACTGAGTAA-3′; No. 8, 5′-TTGGATTGACC-TTCTAGTCAA-3′ (QIAGEN), and Dharmacon SmartPool L-022219-00 (Thermo Fisher Scientific). Sgo2 and B56α were depleted using Dharmacon SmartPools L-016154-01 and L-009352-00, respectively, and HURP and CenpE were targeted with 5′-TACTTTGAATTCACAAACTAA-3′ and 5′-CACGATACTGTTAACATGAAT-3′, respectively (QIAGEN).

Mitotic chromosome spreads
HeLa S3 cells were treated with Gl2, astrin, HURP, Sgo1, or Sgo2 siRNA oligonucleotides for 48 h or kinastrin/SKAP siRNA for 72 h. 100 ng/ml nocodazole was added to the control cells 14 h before harvesting. Mitotic cells were collected by mitotic shake-off, and chromosome spreads were prepared as described previously (Thein et al., 2007).

Image acquisition and time-lapse microscopy
Cells were processed for immunofluorescence analysis as described previously (Thein et al., 2007). For MT plus end staining, cells were fixed with methanol for 5 min at −20°C. Image acquisition was performed on an upright microscope (BX61; Olympus) with Plan-Apochromat 100×/1.4 NA and 60×/1.35 NA oil immersion objective lenses and a CoolSnap HQ2 camera (Roper Industries) under the control of MetaMorph 7.5 software (Molecular Devices). Image stacks were deconvolved using MetaMorph software. For live cell imaging, cells were plated in 35-mm dishes with a 14-mm 1.5 thickness coverglass window on the bottom (MatTek), then placed in a 37°C, 5% CO₂ environmental chamber on the microscope stage of a spinning disc confocal system (Ultraview Vox; Perkin Elmer). Imaging was performed using a 60× 1.4 NA oil immersion objective lens.

with control or siKinastrin oligos for 72 h, then stained for EB1 and kinastrin. Boxed regions are shown enlarged on the right. (G) MT polymerization in the presence of buffer, taxol, GST, or GST–kinastrin at the indicated concentrations was followed in a fluorimeter. Each curve is representative of three independent experiments. (H) HeLa cells were treated overnight with 200 µM monastrol followed by 1 h cold treatment on ice. MT regrowth was initiated by the addition of fresh 37°C medium then monitored for 45 min by staining for astrin, tubulin, and DNA (DAPI). (I) HeLa cells treated with control, Nuf2, or kinastrin siRNA oligos for 72 h were cold treated for 10 min to visualize stable kinetochore fibers. The bottom row shows enlarged views of the boxed regions. Bars, 10 µm unless otherwise indicated.

Cells were typically imaged every minute for 12 h, acquiring z stacks containing 29 steps, 0.6 µm apart, with 2% laser power and 30 ms exposure. For MT plus end imaging, cells were imaged every 1.25 or 3.2 s for 1.5 min, acquiring z stacks with 6 steps, 0.4 µm apart. Maximum intensity projections of the fluorescent channels were performed using Volocity (PerkinElmer). Images were cropped in Photoshop CS3 (Adobe) or ImageJ (National Institutes of Health) and transferred into Illustrator CS3 (Adobe) to produce figures.

MT polymerization assay
Tubulin polymerization was measured by fluorescence enhancement because of the incorporation of a fluorescent dye into the tubulin polymers using a tubulin polymerization kit (Cytoskeleton, Inc.). Fluorescence emission at 460 nm was followed for 1 h at 37°C with one reading per minute using a fluorimeter (Berthold Technologies).

Online supplemental material
Fig. S1 describes the characterization of the GFP–astrin cell line, sheep anti-astrin antibodies, and C15orf23 siRNA duplexes. Figs. S2 and S3 show that perturbing the astrin–kinastrin complex results in loss of centrosome cohesion but does not affect the shugoshin pathway required for centromeric cohesin protection. Videos 1–7 show spindle formation and chromosome alignment in control, astrin-depleted, and kinastrin-depleted cells passing through mitosis. In Videos 8 and 9, MT plus end tracking of GFP–astrin alone and GFP–astrin and EB1-mCherry together is followed.

References

Akhmanova, A., and M.O. Steinmetz. 2008. Tracking the ends: a dynamic protein network controls the fate of microtubule tips. *Nat. Rev. Mol. Cell Biol.* 9:309–322. doi:10.1038/nrm2369

Bader, J.R., and K.T. Vaughan. 2010. Dynein at the kinetochore: timing, interactions and functions. *Semin. Cell Dev. Biol.* 21:269–275. doi:10.1016/j.semcdb.2009.12.015

Barisic, M., B. Sohm, P. Mikolcevic, C. Wandke, V. Rauch, T. Ringer, M. Hess, G. Bonn, and S. Geley. 2010. Spindly/CCDC99 is required for efficient chromosome congression and mitotic checkpoint regulation. *Mol. Biol. Cell.* 21:1968–1981. doi:10.1091/mbc.E09-04-0356

Bastos, R.N., and F.A. Barr. 2010. Plk1 negatively regulates Cep55 recruitment to the midbody to ensure orderly abscission. *J. Cell Biol.* 191:751–760. doi:10.1083/jcb.201008108

Chan, Y.W., L.L. Fava, A. Uldschmid, M.H. Schmitz, D.W. Gerlich, E.A. Nigg, and A. Santamaria. 2009. Mitotic control of kinetochore-associated dynein and spindle orientation by human Spindly. *J. Cell Biol.* 185:859–874. doi:10.1083/jcb.200812167

Cheeseman, I.M., and A. Desai. 2008. Molecular architecture of the kinetochore-microtubule interface. *Nat. Rev. Mol. Cell Biol.* 9:33–46. doi:10.1038/nrm2310

Cheeseman, I.M., J.S. Chappie, E.M. Wilson-Kubalek, and A. Desai. 2006. The conserved KMN network constitutes the core microtubule-binding site of the kinetochore. *Cell.* 127:983–997. doi:10.1016/j.cell.2006.09.039

Cox, J., and M. Mann. 2008. MaxQuant enables high peptide identification rates, individualized p.p.b.-range mass accuracies and proteome-wide protein quantification. *Nat. Biotechnol.* 26:1367–1372. doi:10.1038/nbt.1511

Daum, J.R., J.D. Wren, J.J. Daniel, S. Sivakumar, J.N. McAvoy, T.A. Potapova, and G.J. Gorbsky. 2009. Ska3 is required for spindle checkpoint silencing and the maintenance of chromosome cohesion in mitosis. *Curr. Biol.* 19:1467–1472. doi:10.1016/j.cub.2009.07.017

Echeverri, C.J., B.M. Paschal, K.T. Vaughan, and R.B. Vallee. 1996. Molecular characterization of the 50-kD subunit of dynactin reveals function for the complex in chromosome alignment and spindle organization during mitosis. *J. Cell Biol.* 132:617–633. doi:10.1083/jcb.132.4.617

Fang, L., A. Seki, and G. Fang. 2009. SKAP associates with kinetochores and promotes the metaphase-to-anaphase transition. *Cell Cycle.* 8:2819–2827. doi:10.4161/cc.8.17.9514

Gassmann, R., A.J. Holland, D. Varma, X. Wan, F. Civril, D.W. Cleveland, K. Oegema, E.D. Salmon, and A. Desai. 2010. Removal of Spindly from microtubule-attached kinetochores controls spindle checkpoint silencing in human cells. *Genes Dev.* 24:957–971. doi:10.1101/gad.1886810

Kitajima, T.S., T. Sakuno, K. Ishiguro, S. Iemura, T. Natsume, S.A. Kawashima, and Y. Watanabe. 2006. Shugoshin collaborates with protein phosphatase 2A to protect cohesin. *Nature.* 441:46–52. doi:10.1038/nature04663

Kobayashi, T., and T. Murayama. 2009. Cell cycle-dependent microtubule-based dynamic transport of cytoplasmic dynein in mammalian cells. *PLoS ONE.* 4:e7827. doi:10.1371/journal.pone.0007827

Koffa, M.D., C.M. Casanova, R. Santarella, T. Köcher, M. Wilm, and I.W. Mattaj. 2006. HURP is part of a Ran-dependent complex involved in spindle formation. *Curr. Biol.* 16:743–754. doi:10.1016/j.cub.2006.03.056

Maffini, S., A.R. Maia, A.L. Manning, Z. Maliga, A.L. Pereira, M. Junqueira, A. Shevchenko, A. Hyman, J.R. Yates III, N. Galjart, et al. 2009. Motor-independent targeting of CLASPs to kinetochores by CENP-E promotes microtubule turnover and poleward flux. *Curr. Biol.* 19:1566–1572. doi:10.1016/j.cub.2009.07.059

Manning, A.L., S.F. Bakhoum, S. Maffini, C. Correia-Melo, H. Maiato, and D.A. Compton. 2010. CLASP1, astrin and Kif2b form a molecular switch that regulates kinetochore-microtubule dynamics to promote mitotic progression and fidelity. *EMBO J.* 29:3531–3543. doi:10.1038/emboj.2010.230

McEwen, B.F., and Y. Dong. 2010. Contrasting models for kinetochore microtubule attachment in mammalian cells. *Cell. Mol. Life Sci.* 67:2163–2172. doi:10.1007/s00018-010-0322-x

Ohta, S., J.C. Bukowski-Wills, L. Sanchez-Pulido, Fde.L. Alves, L. Wood, Z.A. Chen, M. Platani, L. Fischer, D.F. Hudson, C.P. Ponting, et al. 2010. The protein composition of mitotic chromosomes determined using multiclassifier combinatorial proteomics. *Cell.* 142:810–821. doi:10.1016/j.cell.2010.07.047

Pfister, K.K., E.M. Fisher, I.R. Gibbons, T.S. Hays, E.L. Holzbaur, J.R. McIntosh, M.E. Porter, T.A. Schroer, K.T. Vaughan, G.B. Witman, et al. 2005. Cytoplasmic dynein nomenclature. *J. Cell Biol.* 171:411–413. doi:10.1083/jcb.200508078

Pfister, K.K., P.R. Shah, H. Hummerich, A. Russ, J. Cotton, A.A. Annuar, S.M. King, and E.M. Fisher. 2006. Genetic analysis of the cytoplasmic dynein subunit families. *PLoS Genet.* 2:e1. doi:10.1371/journal.pgen.0020001

Santaguida, S., and A. Musacchio. 2009. The life and miracles of kinetochores. *EMBO J.* 28:2511–2531. doi:10.1038/emboj.2009.173

Sauer, G., R. Körner, A. Hanisch, A. Ries, E.A. Nigg, and H.H. Silljé. 2005. Proteome analysis of the human mitotic spindle. *Mol. Cell. Proteomics.* 4:35–43.

Schmidt, J.C., T. Kiyomitsu, T. Hori, C.B. Backer, T. Fukagawa, and I.M. Cheeseman. 2010. Aurora B kinase controls the targeting of the Astrin-SKAP complex to bioriented kinetochores. *J. Cell Biol.* 191:269–280. doi:10.1083/jcb.201006129

Shevchenko, A., M. Wilm, O. Vorm, and M. Mann. 1996. Mass spectrometric sequencing of proteins silver-stained polyacrylamide gels. *Anal. Chem.* 68:850–858. doi:10.1021/ac950914h

Silljé, H.H., S. Nagel, R. Körner, and E.A. Nigg. 2006. HURP is a Ran-importin beta-regulated protein that stabilizes kinetochore microtubules in the vicinity of chromosomes. *Curr. Biol.* 16:731–742. doi:10.1016/j.cub.2006.02.070

Thein, K.H., J. Kleylein-Sohn, E.A. Nigg, and U. Gruneberg. 2007. Astrin is required for the maintenance of sister chromatid cohesion and centrosome integrity. *J. Cell Biol.* 178:345–354. doi:10.1083/jcb.200701163

Uhlmann, F., D. Wernic, M.A. Poupart, E.V. Koonin, and K. Nasmyth. 2000. Cleavage of cohesin by the CD clan protease separin triggers anaphase in yeast. *Cell.* 103:375–386. doi:10.1016/S0092-8674(00)00130-6

Varma, D., P. Monzo, S.A. Stehman, and R.B. Vallee. 2008. Direct role of dynein motor in stable kinetochore-microtubule attachment, orientation, and alignment. *J. Cell Biol.* 182:1045–1054. doi:10.1083/jcb.200710106

Whitfield, M.L., G. Sherlock, A.J. Saldanha, J.I. Murray, C.A. Ball, K.E. Alexander, J.C. Matese, C.M. Perou, M.M. Hurt, P.O. Brown, and D. Botstein. 2002. Identification of genes periodically expressed in the human cell cycle and their expression in tumors. *Mol. Biol. Cell.* 13:1977–2000. doi:10.1091/mbc.02-02-0030.

Zeng, K., R.N. Bastos, F.A. Barr, and U. Gruneberg. 2010. Protein phosphatase 6 regulates mitotic spindle formation by controlling the T-loop phosphorylation state of Aurora A bound to its activator TPX2. *J. Cell Biol.* 191:1315–1332. doi:10.1083/jcb.201008106